Topological charge and cooling scales in pure SU(2) lattice gauge theory

Bernd A. Berg and David A. Clarke
Department of Physics, Florida State University, Tallahassee, Florida 32306-4350, USA

(Received 15 October 2017; revised manuscript received 11 February 2018; published 15 March 2018; corrected 3 April 2019)

Using Monte Carlo simulations with overrelaxation, we have equilibrated lattices up to $\beta = 2.928$, size 60^4, for pure SU(2) lattice gauge theory with the Wilson action. We calculate topological charges with the standard cooling method and find that they become more reliable with increasing β values and lattice sizes. Continuum limit estimates of the topological susceptibility χ are obtained of which we favor $\chi^{1/4}/T_c = 0.643(12)$, where T_c is the SU(2) deconfinement temperature. Differences between cooling length scales in different topological sectors turn out to be too small to be detectable within our statistical errors.

DOI: 10.1103/PhysRevD.97.054506

I. INTRODUCTION

Since Lüscher proposed the gradient flow method [1], the topic of scale setting has received increased attention. See, for instance, the review [2]. In [3] Bonati and D'Elia suggested replacing the gradient flow by the computationally more efficient standard cooling flow [4] and supported this idea with numerical evidence for pure SU(3) lattice gauge theory (LGT). In a recent large statistics study of pure SU(2) LGT [5], we investigated the approach to the continuum limit for six gradient and six cooling scales. They are distinguished by the use of three different energy operators and two different ways of setting the initial scaling to agree with the deconfining scale on small lattices. We studied systematic errors of scale setting which, although they are only about 1% for our largest lattices at $\beta \approx 2.9$ (2% at $\beta \approx 2.6$), dominate the statistical errors. Quantitatively gradient and cooling scales worked equally well, with differences between the six scales within the cooling and within the gradient group larger than differences between corresponding scales of the two groups. See [6] for a summary.

Using cooling we also calculated the topological charge Q on each of our configurations and showed that our charges of subsequent configurations are statistically independent. This was only done for the cooling flow as it takes less than 1/34 of the CPU time needed for the corresponding gradient flow, while the equivalence of these scales was already demonstrated in [5]. Here we supplement our previous publication by presenting details of our calculations of Q, and adding a considerable number of additional lattices at large β so that we can estimate finite size corrections of the topological susceptibility, and come up with a continuum limit extrapolation.

We investigate whether there are noticeable differences in cooling scales when we restrict them to fixed topological sectors. Although fixed topological sectors imply for local operators only a bias of order $1/V$ [7,8], getting trapped in a topological charge sector has often been a reason of concern. For instance, Lüscher and Schaefer [9] proposed to bypass the problem by imposing open boundary conditions in one of the lattice directions. Recently Lüscher [10] emphasized that master-field configurations on very large lattices would alleviate topological freezing. We find that the lattices used in our SU(2) investigation are so large that the $1/V$ effects due to topological freezing are swallowed by statistical errors.

In the next section we discuss our data for the topological charge. In Sec. III we present cooling scales and our continuum extrapolation of the topological susceptibility. In Sec. IV we search for correlations of topological charge sectors with differences in the considered cooling scales. Summary and conclusions are given in Sec. V.

II. TOPOLOGICAL CHARGE

The continuum equation of the topological charge,

$$Q = \frac{g^2}{16\pi^2} \int d^4x \mathrm{Tr}\ {}^*F_{\mu\nu} F^{\mu\nu}, \tag{1}$$

where ${}^*F$ is the dual field strength tensor, translates on the lattice to the discretization

$$Q_L = \sum_n q_L(n), \tag{2}$$

Published by the American Physical Society under the terms of the Creative Commons Attribution 4.0 International license. Further distribution of this work must maintain attribution to the author(s) and the published article's title, journal citation, and DOI. Funded by SCOAP³.

where the sum is over all lattice sites and

$$q_L(n) = -\frac{1}{2^9\pi^2}\sum_{\mu\nu\rho\sigma=\pm1}^{\pm4}\tilde{\epsilon}_{\mu\nu\rho\sigma}\mathrm{Tr}U^{\square}_{\mu\nu}(n)U^{\square}_{\rho\sigma}(n). \quad (3)$$

Here $\tilde{\epsilon} = \epsilon$ for positive indices while $\tilde{\epsilon}_{\mu\nu\rho\sigma} = -\tilde{\epsilon}_{(-\mu)\nu\rho\sigma}$ for negative indices.

Measurements of this quantity on MC-generated lattice configurations suffer from lattice artifacts, which we suppressed by cooling. A SU(2) cooling step minimizes the action locally by replacing a link variable $U_\mu(x)$ by a function of the staple matrix $U^{\sqcup}_\mu(x)$:

$$U_\mu(x) \to U'_\mu(x) \equiv \frac{U^{\sqcup}_\mu(x)}{\sqrt{\det U^{\sqcup}_\mu(x)}}. \quad (4)$$

After sufficiently many cooling sweeps one may reach (and does on large enough lattices) metastable configurations to which a topological charge can be assigned. Picking a suitable number m_c of cooling sweeps, the obtained charge values still suffer from discretization errors, which can be absorbed by multiplicative normalization constants N_L, replacing $Q^{m_c}_L$ by

$$Q^{m_c} = N^{m_c}_L Q^{m_c}_L, \qquad Q^{m_c}_0 = \mathrm{nint}(Q^{m_c}), \quad (5)$$

where nint stands for nearest integer and we calculate the constants $N^{m_c}_L$ following the procedure most clearly explained in Ref. [3] and there attributed to [11]. We minimize the equation

$$\sum_{\mathrm{conf}}\{N^{m_c}_L Q^{m_c}_L(\mathrm{conf}) - \mathrm{nint}[N^{m_c}_L Q^{m_c}_L(\mathrm{conf})]\}^2, \quad (6)$$

where the sum is over all configurations for a fixed lattice size and β value. The integer values $Q^{m_c}_0$ protect the thus defined topological charge against renormalization.

All our lattices are of size N^4. Table I gives an overview of our largest lattices at the β values for which we calculated the topological charge distribution. For each parameter value we generated 128 configurations separated by a sufficiently large number of Monte Carlo overrelaxation (MCOR) sweeps so that they are effectively statistically independent. Each MCOR update consists of one heatbath followed by two overrelaxation updates. For lattice sizes up to 52^4 the statistics is the one of Ref. [5]. For our new, largest lattice, 60^4 at $\beta = 2.928$, lattice configurations are separated by 3×2^{12} MCOR sweeps after 2^{15} sweeps for equilibration.

TABLE I. Overview of our largest N^4 lattices at fixed β values.

N	β	N_L^{100}	N_L^{1000}	N_L^{2048}	$\lvert Q^{2048}_{\max}(1000)\rvert$	% stable	$\lvert Q^{2048}_{\max}(2048)\rvert$
16	2.300	1.202	1.178	1.155	6	61.7	3
28	2.430	1.258	1.128	1.129	15	60.9	13
28	2.510	1.148	1.127	1.124	14	66.4	10
40	2.574	1.159	1.117	1.113	17	58.6	16
40	2.620	1.135	1.111	1.110	13	78.1	12
40	2.670	1.131	1.110	1.108	10	83.6	10
40	2.710	1.131	1.107	1.105	7	87.5	7
40	2.751	1.113	1.108	1.108	8	94.5	8
44	2.816	1.111	1.105	1.101	7	89.1	7
52	2.875	1.112	1.100	1.098	7	96.9	6
60	2.928	1.106	1.107	1.097	5	96.1	5

On each lattice configuration we performed 2048 cooling sweeps and applied the minimization (6) with the charges defined at $m_c = 100$, $m_c = 1000$, and $m_c = 2048$. The corresponding multiplicative constants $N^{m_c}_L$ amount to corrections in the range from up to 26% down to about 10% for our largest lattices and β values, where there is also little m_c dependence of $N^{m_c}_L$. Subsequently, we considered plots of the 3×128 time series for the topological charge that we created for the different m_c values. For $m_c = 2048$ examples of these plots for increasing β values and lattice sizes are shown in Figs. 1, 2, 3, 4. We plot $Q^{2048}(i_c)$, i_c number of cooling sweeps, instead of the integer valued charges $Q^{2048}_0(i_c)$, because the latter would obscure how good the mapping on integer values really is. Apart from that, using the integer values $Q^{m_c}_0(i_c)$ in our subsequent analysis would lead to the same conclusions.

As discussed in [12], when approaching the continuum limit the topological charge has to be defined at a *fixed*,

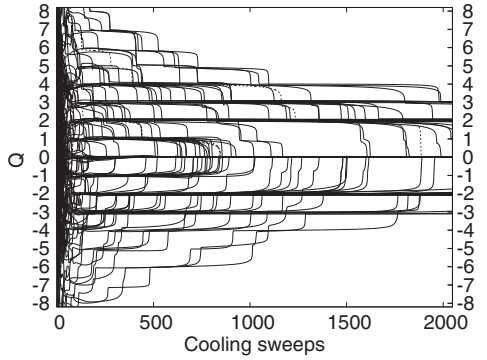

FIG. 1. 16^4, $\beta = 2.3$: Cooling time series $Q^{2048}(i_c)$.

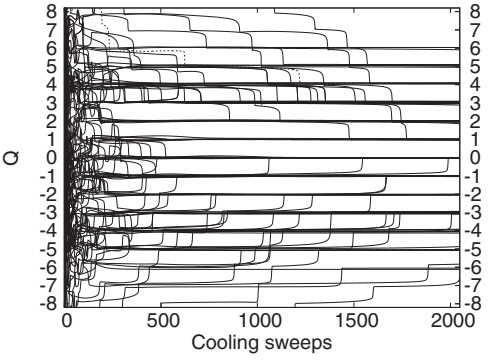

FIG. 2. 28^4, $\beta = 2.51$: Cooling time series $Q^{2048}(i_c)$.

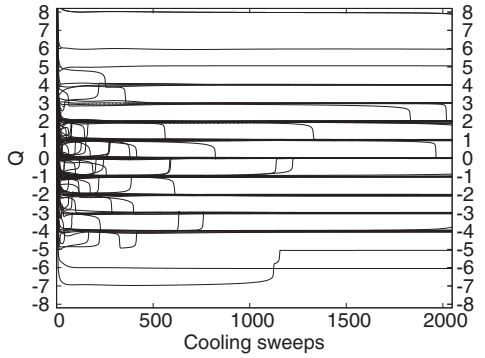

FIG. 3. 40^4, $\beta = 2.751$: Cooling time series $Q^{2048}(i_c)$.

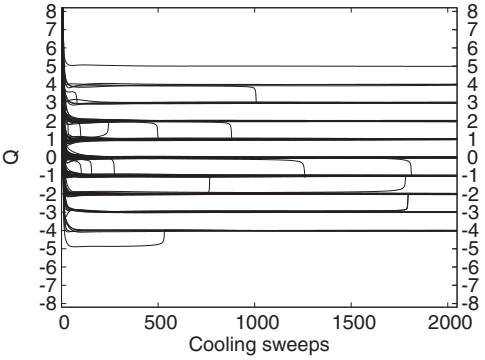

FIG. 4. 60^4, $\beta = 2.928$: Cooling time series $Q^{2048}(i_c)$.

large enough number n_c of cooling sweeps. This number can agree with the number m_c used for the minimization (6), but needs not necessarily be identical. So our charges have two labels:

$$Q = Q^{m_c}(n_c). \tag{7}$$

For our first two figures a good choice of n_c appears not to exist, because there are a considerable number of transitions between topological sectors over the entire times series range considered, and for the 16^4 lattice the ultimate topological sector $Q = 0$ is approached all the way. In contrast to that we find for Figs. 3 and 4 over a large range of n_c values, certainly including $n_c = 1000$, only few transitions. Also the removal of dislocations by an initial number of cooling of sweeps becomes easier for increasing β. Metastable configurations are not only more stable than at lower β values, but are also reached earlier. In the % stable column of Table I we report the stability of charge sectors under the next 1048 cooling sweeps after $n_c = 1000$. Starting from about $\beta = 2.574$ we see, up to statistical fluctuations, a gradually improving trend with increasing β. If one desires that roughly 90% of configurations are metastable, we must require $\beta \gtrsim 2.75$ and lattices large enough to accommodate physical instantons (their size increases proportionally to our length scales of [5], to which the largest lattice sizes are already adjusted).

The number $n_c = 1000$ is considerably larger than what we would have expected from previous literature. For instance, in Fig. 3 of [3] the topological charge on a 20^4 SU(3) lattice at $\beta = 6.2$ is defined after 21 cooling sweeps. This led us in [5] to work with $n_c = 100$ to define Q^{n_c}. For the purpose of checking the statistical independence of our configurations this is still sufficient, because including some dislocations adds only some statistical noise to the charge correlations. Early SU(2) investigations were performed for such small β values and lattice sizes [13,14] that only qualitative insights could be obtained, as already noted in the paper by Teper [13].

We checked that our $Q^{2048}(1000)$ charges are statistically independent, and that their charge distribution is symmetric under $Q^{2048}(1000) \to -Q^{2048}(1000)$ within statistical errors. For the lattices of Table I histograms of $|Q^{2048}(1000)|$ are compiled in Table II. Table I also compares the largest value of $|Q^{2048}(1000)|$ with the largest value of $|Q^{2048}(2048)|$, and the $|Q^{2048}_{\max}|$ values become quite stable for $\beta \geq 2.574$.

III. COOLING SCALES AND TOPOLOGICAL SUSCEPTIBILITY

To investigate the scaling behavior of the topological susceptibility, we have considerably extended our previous statistics by adding a new 60^4 lattice at $\beta = 2.928$ and

TABLE II. Histograms of $|Q^{2048}(1000)|$ for the β values and lattices of Table I.

β	0	1	2	3	4	5	6	7	8	9	10	11	12	13	14	15	17
2.300	57	4	36	20	6	4	1	0	0	0	0	0	0	0	0	0	0
2.430	6	22	15	15	22	10	10	5	7	7	2	2	1	2	0	2	0
2.510	11	21	17	23	19	17	7	3	1	5	2	1	0	0	1	0	0
2.574	11	12	19	14	14	12	10	12	5	2	5	6	3	0	2	0	1
2.620	13	18	23	19	13	13	7	5	2	3	5	3	3	1	0	0	0
2.670	12	28	31	11	15	12	9	3	3	3	1	0	0	0	0	0	0
2.710	20	30	33	23	11	7	3	1	0	0	0	0	0	0	0	0	0
2.751	28	37	31	16	11	1	2	1	1	0	0	0	0	0	0	0	0
2.816	24	42	32	18	9	1	1	1	0	0	0	0	0	0	0	0	0
2.875	29	40	27	24	5	2	0	1	0	0	0	0	0	0	0	0	0
2.928	26	49	30	12	10	1	0	0	0	0	0	0	0	0	0	0	0

smaller lattices at each β value. Results for the cooling length scales are discussed in the next subsection followed by an analysis of the topological susceptibility in Sec. III B.

A. Cooling length scales

Data for the cooling length scales are compiled in Tables III and IV. For the convenience of the reader we include for each β value the largest lattice, although they can already be found in [5], with the exception of 60^4 at $\beta = 2.928$. The 28^4 lattices at $\beta = 2.620$ and $\beta = 2.670$ are also from [5]. All other lattices are from new simulations. For them we did not calculate the gradient length scales, because the gradient flow takes at least 34 times more CPU time than the cooling flow.

Following [5] we use for the calculation of the length scales three definitions of the energy density: $E_0(t)$, $E_1(t)$, and $E_4(t)$. $E_0(t)$ is the Wilson action up to a constant factor, $E_1(t)$ is the sum of the squared Pauli matrices of the plaquette variables, and $E_4(t)$ is Lüscher's [1] energy density which averages over the four plaquettes attached to each site n in a fixed $\mu\nu$, $\mu \neq \nu$ plane. The functions

$$y_i(t) = t^2 E_i(t), \qquad (i = 0, 1, 4) \tag{8}$$

are used to set up three cooling scales by choosing appropriate fixed target values y_i^0 and performing cooling steps (4) until $y_i^0 = (t_i^0)^2 E_i(t_i^0)$ is reached. As a function of β, the observable

$$s_i^0(\beta) = \sqrt{t_i^0(\beta)} \tag{9}$$

then scales like a length.

There is some ambiguity in the choice of target values. In [5] they are chosen so that either (superscripts 01) initial estimates of the scales s_0^{01} and s_1^{01} (they give almost identical values) agree with the deconfinement scaling from $\beta \approx 2.3$ on a 4×8^3 lattice to $\beta \approx 2.44$ on a 6×12^3 lattice, or so that (superscripts 02) s_4^{02} agrees. This leads to two possible values per energy observable, i.e., a total of six targets:

$$y_0^{01} = 0.0440, \quad y_1^{01} = 0.0430, \quad y_4^{01} = 0.0350, \tag{10}$$

TABLE III. Cooling length scales for the y_i^{01} set. The * denotes lattices that are too small to be used for finite size fits. TVNR stands for "target value not reached".

β	N	$L_7 = s_0^{01}$	$L_8 = s_1^{01}$	$L_9 = s_4^{01}$
2.300	16	1.3433(24)	1.3385(23)	1.2575(74)
2.430	28	2.0892(28)	2.0707(28)	1.9446(95)
2.510	28	2.7522(68)	2.7267(66)	2.548(15)
2.574*	16	3.512(48)	3.478(47)	3.309(48)
2.574	28	3.422(13)	3.390(13)	3.168(18)
2.574	40	3.4048(69)	3.3730(67)	3.137(17)
2.620*	16	4.55(14)	4.50(26)	4.28(12)
2.620	28	3.9752(19)	3.915(19)	3.690(24)
2.620	40	3.9509(95)	3.913(93)	3.645(22)
2.670*	16	6.28(36)	6.23(36)	5.88(38)
2.670	28	4.676(32)	4.631(31)	4.314(39)
2.670	40	4.618(17)	4.574(16)	4.298(26)
2.710*	16	8.03(76)	7.96(80)	7.67(1.3)
2.710	28	5.232(41)	5.184(40)	4.829(47)
2.710	40	5.203(21)	5.154(21)	4.794(28)
2.751*	16	TVNR	TVNR	TVNR
2.751	28	5.880(82)	5.824(78)	5.487(74)
2.751	40	5.913(32)	5.857(32)	5.434(40)
2.816	28	8.247(27)	8.167(26)	7.561(25)
2.816	40	7.089(58)	7.021(58)	6.517(68)
2.816	44	7.105(45)	7.039(45)	6.511(55)
2.875*	28	12.84(84)	12.06(83)	11.70(84)
2.875	40	8.55(11)	8.464(10)	7.885(97)
2.875	44	8.637(93)	8.554(92)	7.912(89)
2.875	52	8.514(60)	8.433(59)	7.825(68)
2.928*	28	16.3(1.8)	16.2(1.8)	14.8(1.7)
2.928	40	10.90(30)	10.79(29)	9.89(27)
2.928	44	10.01(16)	9.92(16)	9.18(14)
2.928	52	9.940(88)	9.846(87)	9.112(93)
2.928	60	9.835(67)	9.742(66)	9.053(70)

TABLE IV. Cooling length scales for the y_i^{02} set. The * denotes lattices that are too small to be used for finite size fits. TVNR stands for "target value not reached".

β	N	$L_{10} = s_0^{02}$	$L_{11} = s_1^{02}$	$L_{12} = s_4^{02}$
2.300	16	1.8307(39)	1.8282(39)	1.728(10)
2.430	28	2.7317(43)	2.7212(42)	2.565(12)
2.510	28	3.552(10)	3.5371(99)	3.315(18)
2.574	16	4.550(69)	4.529(65)	4.323(71)
2.574	28	4.405(20)	4.386(29)	4.123(25)
2.574	40	4.377(11)	4.358(10)	4.074(20)
2.620*	16	5.82(17)	5.80(17)	5.58(17)
2.620	28	5.104(31)	5.082(31)	4.787(35)
2.620	40	5.068(15)	5.045(15)	4.725(26)
2.670	16	7.92(54)	7.89(54)	7.57(53)
2.670	28	6.021(46)	5.993(46)	5.603(58)
2.670	40	5.910(25)	5.884(25)	5.536(33)
2.710*	16	9.88(2.3)	9.86(2.3)	9.72(2.1)
2.710	28	6.675(58)	6.645(57)	6.228(67)
2.710	40	6.656(31)	6.626(30)	6.188(38)
2.751*	16	TVNR	TVNR	TVNR
2.751	28	7.55(13)	7.52(13)	7.07(11)
2.751	40	7.576(46)	7.541(46)	7.038(54)
2.816	28	10.48(35)	10.44(35)	9.72(34)
2.816	40	9.076(84)	9.034(84)	8.426(92)
2.816	44	9.056(65)	9.015(64)	8.349(73)
2.875*	28	14.66(92)	14.62(92)	14.26(96)
2.875	40	10.98(16)	10.93(16)	10.21(16)
2.875	44	11.11(15)	11.06(15)	10.29(15)
2.875	52	10.879(87)	10.830(86)	10.122(92)
2.928*	28	20.3(2.3)	20.0(2.3)	17.4(2.0)
2.928	40	13.99(42)	13.92(42)	12.87(40)
2.928	44	12.78(23)	12.72(23)	11.82(21)
2.928	52	12.72(13)	12.67(13)	11.76(13)
2.928	60	12.561(97)	12.503(96)	11.653(95)

$$y_0^{02} = 0.0822, \quad y_1^{02} = 0.0812, \quad y_4^{02} = 0.0656. \tag{11}$$

The numeration of the scales as L_7 to L_{12} follows the convention of [5], where L_1 to L_6 are the corresponding gradient scales.

B. Topological susceptibility

At each β and lattice size, we calculated the topological susceptibility

$$\chi = \frac{1}{n}\frac{1}{N^4}\sum_{i=1}^{n}\langle Q_i^2\rangle, \tag{12}$$

where the sum runs over our $n = 128$ configurations at two fixed (m_c, n_c) values,

$$n_c = m_c = 100 \quad \text{and} \quad n_c = m_c = 1000. \tag{13}$$

Results for $\chi^{1/4}$ with jackknife error bars are given in Table V. For $\beta \to \infty$ the product of $\chi^{1/4}$ with one of our cooling length scales should approach a constant up to a^2 corrections (a lattice spacing). As in Figs. 7, 8 and 10 of Ref. [5] we choose the L_{10} length scale as our reference and report in Table V estimates of $L_{10}\chi^{1/4}$. The quantities cannot simply be obtained by multiplying the L_{10} values of Table IV with the $\chi^{1/4}$ estimates of Table V and using error propagation, because their values come from the same configurations. Instead 128 jackknife bins were calculated for the product $L_{10}\chi^{1/4}$ at each fixed lattice size and β value. The given error bars are from these jackknife bins.

Figure 5 shows the time evolution of $L_{10}\chi^{1/4}$ for the same lattice sizes and β values that we used to exhibit the time evolution of the topological charge in Figs. 1–4. There are three almost constant lines near the top of Fig. 5: A red line and two blue lines that fall practically on top of one another. The red line and one of the blue lines belong to the 60^4 lattice at $\beta = 2.928$ used for Fig. 4. Red curves are to be read using the bottom abscissa with error bars plotted every 100 cooling sweeps, while blue curves are to be read using the top abscissa with error bars plotted every 10 sweeps. For the 60^4 lattice the blue line stays constant and the red line continues this out to 2048 cooling sweeps.

We do not include the cooling time series for the 40^4 lattice at $\beta = 2.751$ in Fig. 5, because they fall on top of the time series of the 60^4 lattice at $\beta = 2.928$.

Next we consider $L_{10}\chi^{1/4}$ from the 28^4 lattice at $\beta = 2.51$ under cooling, given by the topmost, decreasing red curve. As one may have expected from the time evolution of the topological charge in Fig. 2, its susceptibility decreases monotonically. However, the behavior of the scale during the first 200 cooling sweeps comes as a surprise. It is given by a second blue line that falls almost on top of the blue line for $L_{10}\chi^{1/4}$ from the 60^4 lattice at $\beta = 2.928$. In Fig. 2 there are many transitions between topological sectors in this range. So, an almost constant topological susceptibility is only possible when the transitions that increase the topological charge are, within statistical errors, matched by those that decrease it. An enhancement of the first 200

TABLE V. Topological susceptibility defined after 1000 and 100 cooling sweeps respectively. The * denotes lattices that are too small to be used.

		1000		100	
β	N	$\chi^{1/4}$	$L_{10}\chi^{1/4}$	$\chi^{1/4}$	$L_{10}\chi^{1/4}$
2.300	16	0.0903(28)	0.1654(52)	0.1231(35)	0.2253(64)
2.430	28	0.0834(27)	0.2276(72)	0.1023(33)	0.2790(89)
2.510	28	0.0744(25)	0.2642(86)	0.0821(26)	0.2917(90)
2.574*	16	0.0510(37)	0.232(16)	0.0667(21)	0.3033(82)
2.574	28	0.0601(18)	0.2647(77)	0.0653(26)	0.288(11)
2.574	40	0.0609(19)	0.2666(80)	0.0677(21)	0.2963(92)
2.620*	16	0.0291(32)	0.169(17)	0.0562(20)	0.3272(63)
2.620	28	0.0537(16)	0.2740(76)	0.0570(16)	0.2912(79)
2.620	40	0.0557(19)	0.2821(93)	0.0582(19)	0.2950(94)
2.670*	16	0.026(26)	0.21(21)	0.0419(25)	0.332(13)
2.670	28	0.0467(15)	0.2811(81)	0.0477(15)	0.2873(83)
2.670	40	0.0484(16)	0.2860(90)	0.0511(17)	0.3020(96)
2.710*	16	0	0	0.0345(25)	0.341(75)
2.710	28	0.0444(16)	0.2966(97)	0.0460(17)	0.307(11)
2.710	40	0.0404(12)	0.2692(77)	0.0416(13)	0.2772(82)
2.751	28	0.0387(15)	0.2925(96)	0.0399(16)	0.3010(98)
2.751	40	0.0381(15)	0.286(11)	0.0385(15)	0.290(11)
2.816	28	0.0305(15)	0.3195(97)	0.0327(18)	0.343(14)
2.816	40	0.0324(12)	0.294(10)	0.0328(12)	0.298(10)
2.816	44	0.0332(12)	0.3010(96)	0.0336(12)	0.3045(96)
2.875*	28	0.0227(16)	0.333(12)	0.0390(17)	0.3512(94)
2.875	40	0.02748(89)	0.3017(87)	0.02800(96)	0.3074(93)
2.875	44	0.02681(92)	0.2980(92)	0.0270(11)	0.300(11)
2.875	52	0.02760(92)	0.3002(97)	0.02822(93)	0.3070(97)
2.928*	28	0.0173(17)	0.345(12)	0.0173(17)	0.345(14)
2.928	40	0.0235(11)	0.3287(97)	0.0235(11)	0.3286(98)
2.928	44	0.02492(77)	0.3185(75)	0.02534(85)	0.3239(84)
2.928	52	0.02359(81)	0.3002(94)	0.02360(80)	0.3003(93)
2.928	60	0.02297(70)	0.2885(84)	0.02313(72)	0.2906(87)

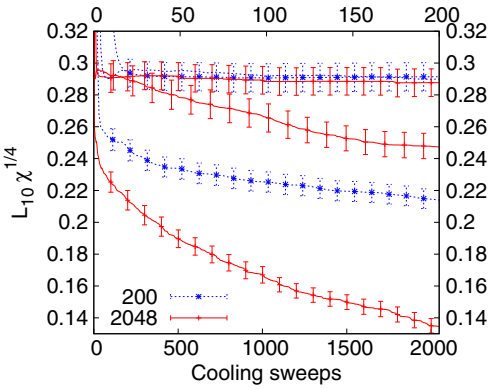

FIG. 5. Cooling time series of $L_{10}\chi^{1/4}$ for 2048 cooling sweeps on the bottom abscissa (for the red curves) and 200 cooling sweeps on the top abscissa (for the blue curves). Lattice parameters are given in the text.

cooling sweeps of Fig. 2 confirms this scenario. Notably, even in the range of less than 200 cooling sweeps $L_{10}\chi^{1/4}$ scales then already very well as a constant all the way from $\beta = 2.51$ to $\beta = 2.928$.

The lowest blue and red curves correspond to the 16^4 lattice at $\beta = 2.3$ that was used for Fig. 1. Both curves are now monotonically decreasing and demonstrate that $\beta = 2.3$ is too small to provide a reliable estimate of the topological susceptibility.

Let us now discuss scaling and continuum limit extrapolation of $\chi^{1/4}$. For this purpose we combine the results for $L_{10}\chi^{1/4}$ at fixed β but different N using two-parameter fits,

$$L_{10}\chi^{1/4}(\beta, N) = a_1 + \frac{a_2}{N^4}, \tag{14}$$

where a_1 serves as an estimator for $L_{10}\chi^{1/4}(\beta)$.

The lattices with * in the first column of Tables III, IV and V turned out to be too small to deliver reliable data and are therefore not included in these fits. For instance, as reported in Table V, at $\beta = 2.71$ the topological susceptibility is zero at $n_c = 1000$ for the 16^4 lattice, implying that the topological charge is zero on each of our 128 configurations. Also the cooling scale breaks down at high β values when the lattice sizes are too small. For the 16^4 lattice this happens for $\beta \geq 2.751$, and is illustrated in Fig. 6. The trajectories for the 40^4 and the 28^4 lattice fall nicely on top of one another, so that in the figure only the color of the second drawn trajectory is left over. However for the 16^4 lattice, the trajectory fails to take off, so that the $y_0^{02} = 0.0822$ target value (11) for L_{10} is never reached.

Carrying out the fit (14) on the remaining lattices yields results consistent with the fitting form. In particular, in order of $\beta = 2.928$, 2.875 and 2.816, the goodness of fit is $q = 0.92$, 0.78 and 0.48 for $n_c = 1000$, and $q = 0.72$, 0.57 and 0.40 for $n_c = 100$. For $\beta = 2.751$, 2.71, 2.67, 2.62 and 2.574 we performed two-parameter fits with only two lattices so that there are no q-values to report. For $\beta = 2.51$, 2.43 and 2.3 the result from the single lattice listed in Table V is taken in each case.

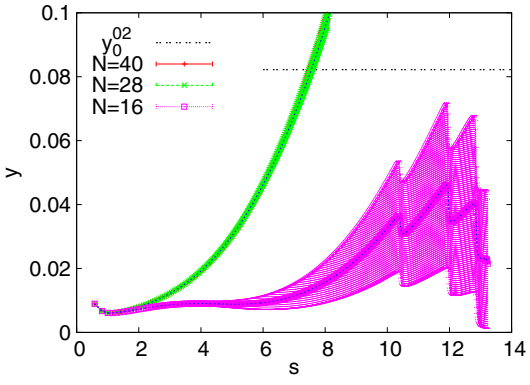

FIG. 6. Cooling trajectories (with error bars) at $\beta = 2.751$ for different lattice sizes. The dashed line indicates the L_{10} target value y_0^{02} (11).

In Fig. 7 we show different fits of the thus obtained data. Using the $L_{10}\chi^{1/4}$ estimates down to $\beta = 2.3$, linear fits to a^2 scaling corrections given by $1/(L_{10})^2$ are shown in the upper part of the figure along with their error bar ranges, while the lower part shows an enhancement. The continuum limit extrapolations are

$$L_{10}\chi^{1/4} = 0.2882(46), \quad q = 0.43 \quad \text{for } n_c = 1000, \tag{15}$$

$$L_{10}\chi^{1/4} = 0.2961(49), \quad q = 0.05 \quad \text{for } n_c = 100. \tag{16}$$

Although the fits to a^2 scaling corrections work well, one may question whether the $L_{10}\chi^{1/4}$ results at $\beta = 2.3$ and 2.43 and to some extent also at $\beta = 2.51$ and 2.574 are really reliable. In short, one could argue in favor or against taking out all β values for which the susceptibility after $n_c = 100$ cooling sweeps is significantly larger than after $n_c = 1000$ cooling sweeps. Taking them out and fitting the remaining points to $L_{10}\chi^{1/4} = \text{constant}$, one obtains the estimates

$$L_{10}\chi^{1/4} = 0.2799(51), \quad q = 0.36 \quad \text{for } n_c = 1000, \tag{17}$$

$$L_{10}\chi^{1/4} = 0.2844(54), \quad q = 0.25 \quad \text{for } n_c = 100. \tag{18}$$

To avoid overloading Fig. 7, the fit to a constant is only indicated for $n_c = 1000$ in the upper part of the figure.

Averaging Eq. (15) with (17), and Eq. (16) with (18), we obtain

$$L_{10}\chi^{1/4} = 0.2841(49) \quad \text{for } n_c = 1000, \tag{19}$$

$$L_{10}\chi^{1/4} = 0.2903(52) \quad \text{for } n_c = 100. \tag{20}$$

To relate $\chi^{1/4}$ to physical scales, we use from Table IX of Ref. [5] the relation $1/T_c = (2.2618 \pm 0.0042)L_{10}$, where T_c is the SU(2) deconfinement temperature in lattice units. Propagating the statistical errors, we obtain from Eqs. (19) and (20)

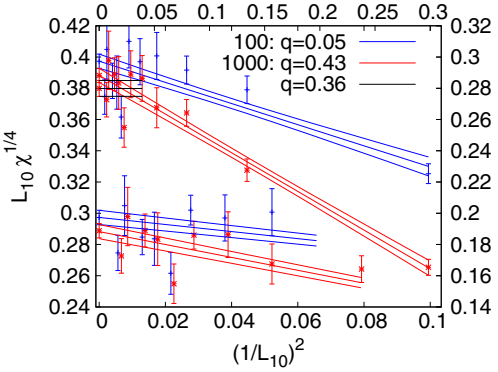

FIG. 7. Scaling of $L_{10}\chi^{1/4}$. The top (bottom) set of fits uses the top (bottom) abscissa and right (left) ordinate.

TABLE VI. Estimates of the topological susceptibility in units of the string tension $\sqrt{\sigma}$.

[Reference] (year)	$\chi^{1/4}/\sqrt{\sigma}$	q_{1000}	q_{100}
[17] (1997)	0.501 (45)	0.32	0.44
[18] (1997)	0.528 (21)	0.00	0.01
[19] (1997)	0.480 (23)	0.32	0.56
[20] (2001)	0.4831 (56)	0.01	0.09
[20] (2001)	0.4745 (63)	0.07	0.40
[20] (2001)	0.4742 (56)	0.06	0.40

$$\chi^{1/4}/T_c = 0.643(12) \quad \text{for } n_c = 1000, \tag{21}$$

$$\chi^{1/4}/T_c = 0.657(12) \quad \text{for } n_c = 100. \tag{22}$$

In the literature $\chi^{1/4}$ for SU(2) LGT has been reported in units of the string tension $\sqrt{\sigma}$. The most accurate estimate of $T_c/\sqrt{\sigma}$ appears to be $T_c/\sqrt{\sigma} = 0.7091(36)$ from Ref. [15], which is consistent with the earlier value $T_c/\sqrt{\sigma} = 0.69(2)$ [16]. Using the former and error propagation our estimates (21) and (22) convert to

$$\chi^{1/4}/\sqrt{\sigma} = 0.4557(83) \quad \text{for } n_c = 1000, \tag{23}$$

$$\chi^{1/4}/\sqrt{\sigma} = 0.4655(88) \quad \text{for } n_c = 100. \tag{24}$$

In Table VI we compile estimates of the literature. The last two columns report Gaussian difference tests obtained by comparing with our estimates (23) and (24). Both of our estimates are lower than each of the others, but this is not surprising since the value for the topological susceptibility goes down with increasing n_c. Our $n_c = 100$ estimate of $\chi^{1/4}/\sqrt{\sigma}$ is statistically already consistent with all but one of the literature. That does not mean that it is a better estimate than that at $n_c = 1000$. Because the previous literature relied on rather small lattice sizes and β values for which only small n_c can be used. It may well be that $n_c = 100$ is too small, and we suggest that our $n_c = 1000$ results (21) and (23) are the best. Although there is a danger of destroying real instantons when the value of n_c is taken too large, there is no evidence for that happening in Fig. 3 or Fig. 4.

IV. SCALES IN TOPOLOGICAL SECTORS

For $\beta \geq 2.71$ we calculated cooling scales on the largest lattice in the topological sectors $Q^{1000} \leq -2$, $Q^{1000} = -1$, $Q^{1000} = 0$, $Q^{1000} = 1$ and $Q^{1000} \geq 2$, and performed student difference tests of each scale with itself on distinct topological sectors. No statistically significant discrepancies are encountered. In particular there are none when comparing the $Q^{1000} < 0$ with the $Q^{1000} > 0$ scales. To increase the statistics for the $|Q^{1000}| \neq 0$ sectors, we combined them into $|Q^{1000}| = 1$ and $|Q^{1000}| \geq 2$. Together with the scales for $Q^{1000} = 0$ their values are listed in Table VII. The scales L_7 and L_8 as well as for L_{10} and L_{11} almost agree because the fluctuations of the operators E_0 and E_1 are strongly correlated and almost identical [5]. So, they are combined in the following.

A histogram of the q values of the remaining $4 \times 15 = 60$ student difference tests for the scales of Table VII is shown in Fig. 8. When the compared data are statistically independent, rely on the same estimator, and are drawn from a Gaussian distribution, the student different tests return uniformly distributed random numbers q in the range $0 < q < 1$, which is consistent with Fig. 8. Furthermore, their mean value comes out to be $\bar{q} = 0.508(40)$ in agreement with the expected 0.5. If there are still some residual correlations between our q-values, this would have decreased the error bar, because the number of independent q would have been counted too high, while each of them still fluctuates like a uniformly distributed random number

TABLE VII. Cooling scales on topological sectors of our largest lattices for $\beta \geq 2.71$.

β	$\lvert Q^{1000}\rvert$	n	L_7	L_8	L_9	L_{10}	L_{11}	L_{12}
2.928	0	26	9.85(15)	9.76(15)	9.07(15)	12.61(23)	12.55(23)	11.66(21)
	1	49	9.93(13)	9.83(13)	9.06(13)	12.74(18)	12.68(17)	11.66(18)
	≥2	53	9.750(92)	9.650(90)	9.040(97)	12.39(14)	12.34(14)	11.64(14)
2.875	0	29	8.64(16)	8.55(16)	7.89(19)	11.16(25)	11.11(25)	10.31(24)
	1	40	8.58(12)	8.50(12)	7.86(12)	11.02(17)	10.97(17)	10.15(18)
	≥2	59	8.416(73)	8.338(72)	7.771(89)	10.68(10)	10.633(99)	10.02(12)
2.816	0	24	7.281(99)	7.212(98)	6.68(12)	9.32(15)	9.27(15)	8.63(16)
	1	42	7.103(75)	7.036(74)	6.540(93)	9.06(12)	9.02(12)	8.41(12)
	≥2	62	7.044(66)	6.979(65)	6.435(80)	8.964(91)	8.924(91)	8.22(11)
2.751	0	28	5.878(70)	5.822(69)	5.381(66)	7.55(11)	7.52(11)	7.006(95)
	1	37	5.895(63)	5.840(62)	5.416(75)	7.542(96)	7.507(95)	7.10(11)
	≥2	63	5.882(43)	5.828(43)	5.382(51)	7.491(61)	7.456(62)	6.920(65)
2.710	0	20	5.277(66)	5.227(65)	4.803(59)	6.750(90)	6.720(90)	6.185(97)
	1	30	5.229(48)	5.179(47)	4.825(73)	6.707(77)	6.676(73)	6.267(92)
	≥2	78	5.175(24)	5.127(24)	4.781(34)	6.615(34)	6.585(34)	6.161(45)

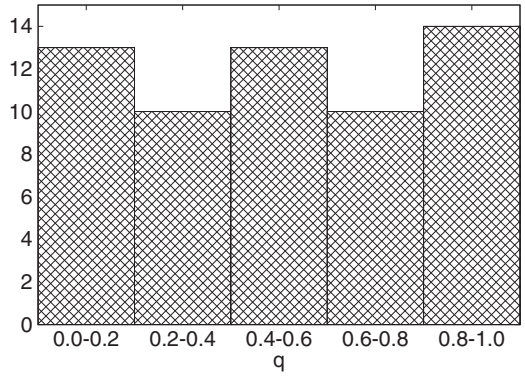

FIG. 8. Histogram of q-values comparing cooling scales from Table VII across topological sectors.

in the interval (0,1). So, we find convincing evidence that the $1/V$ bias expected for our scales due to topological freezing disappears within our statistical noise.

V. SUMMARY AND CONCLUSIONS

Using standard cooling we calculated the topological charge of pure SU(2) LGT for larger lattices and β values than it was done in the literature. For the first time they appear to be large enough to yield stable topological sectors. See Figs. 3–5. From these data we obtain the estimates (21) to (24), which are surprisingly close to previous results of the literature listed in Table VI. This may well be an accident, as the $n_c = 1000$ versus $n_c = 100$ fits of Fig. 7 illustrate.

Within our statistical fluctuations we find no observable correlations between cooling scales (8) and topological charge sectors. Our number of statistically independent configurations is of a typical size as used for scale setting, e.g., [1,9]. So, our results support that the problem of topological freezing only becomes serious when a much higher precision is targeted.

ACKNOWLEDGMENTS

David Clarke was in part supported by the U.S. Department of Energy (DOE) under Contract No. DE-SC0010102. Our calculations used resources of the National Energy Research Scientific Computing Center (NERSC), a DOE Office of Science User Facility supported by the DOE under Contract No. DE-AC02-05CH11231.

[1] M. Lüscher, J. High Energy Phys. 08 (2010) 071; 03 (2014) 092(E).
[2] R. Sommer, *Proc. Sci.*, Lattice2013 (2013) 015.
[3] C. Bonati and M. D'Elia, Phys. Rev. D **89**, 105005 (2014).
[4] B. A. Berg, Phys. Lett. B **104**, 475 (1981).
[5] B. A. Berg and D. A. Clarke, Phys. Rev. D **95**, 094508 (2017).
[6] B. A. Berg and D. A. Clarke, arXiv:1708.08408.
[7] R. Browers, S. Chandrasekharan, J. W. Negele, and U.-J. Wiese, Phys. Lett. B **560**, 64 (2003).
[8] S. Aoki, H. Fukaya, S. Hashimoto, and T. Onogi, Phys. Rev. D **76**, 054508 (2007).
[9] M. Lüscher and S. Schaefer, J. High Energy Phys. 07 (2011) 036.
[10] M. Lüscher, arXiv:1707.09758.
[11] L. Del Debbio, H. Panagopoulos, and E. Vicari, J. High Energy Phys. 08 (2002) 044.
[12] E. Vicari and H. Panagopoulos, Phys. Rep. **470**, 93 (2009).
[13] M. Teper, Phys. Lett. B **171**, 86 (1986).
[14] E.-M. Ilgenfritz, M. L. Laursen, M. Müller-Preußker, G. Schierholz, and H. Schiller, Nucl. Phys. **B268**, 693 (1986).
[15] B. Lucini, M. Teper, and U. Wenger, J. High Energy Phys. 01 (2004) 061.
[16] J. Fingberg, U. Heller, and F. Karsch, Nucl. Phys. **B392**, 493 (1993).
[17] P. de Forcrand, M. G. Pérez, and I.-O. Stamatescu, Nucl. Phys. **B499**, 409 (1997).
[18] T. DeGrand, A. Hasenfratz, and T. G. Kovács, Nucl. Phys. **B505**, 417 (1997).
[19] B. Allés, M. D'Elia, and A. Di Giacomo, Phys. Lett. B **412**, 119 (1997).
[20] B. Lucini and M. Teper, J. High Energy Phys. 06 (2001) 050.

Correction: A minor error in Eq. (23) has been fixed.